Improved selectivity and coke resistance of core-shell alloy catalysts for propane dehydrogenation from first principles and microkinetic analysis

Ling Xiao[a], Fang Ma[a], Yi-An Zhu[a,*], Zhi-Jun Sui[a], Jing-Hong Zhou[a], Xing-Gui Zhou[a], De Chen[b], Wei-Kang Yuan[a]

[a] *UNILAB, State Key Laboratory of Chemical Engineering, Shanghai Key Laboratory of Multiphase Materials Chemical Engineering, East China University of Science and Technology, Shanghai 200237, China*
[b] *Department of Chemical Engineering, Norwegian University of Science and Technology, N-7491 Trondheim, Norway*

ARTICLE INFO

Keywords:
Propane dehydrogenation
Core-shell alloy
DFT
Microkinetic modeling

ABSTRACT

Microkinetic analysis combined with the results obtained from density functional theory calculations has been performed to examine the catalytic activity and selectivity of Pt-based core-shell alloy catalysts for propane dehydrogenation. Calculated results indicate that substitution of 11 late transition metals for the core region of Pt nanoparticles would significantly modify the electronic structure of the surface Pt atoms through the strain effect and charge transfer. The core-shell catalysts are found to have less negative propylene adsorption energies and higher activation energies for the dehydrogenation reactions than Pt, thus giving rise to a lower catalytic activity and a higher selectivity toward propylene. Linear chemisorption energy and transition state energy scaling relations hold very well in the present work, and the adsorption energy of propylene is identified to be a good descriptor to represent the overall kinetics. The scaling relations also suggest that a higher catalyst selectivity toward propylene can only be achieved at the expense of a lower catalytic activity for propane dehydrogenation. If a compromise is made between catalytic activity and catalyst selectivity, Co@Pt is proposed to be the best core-shell catalyst for propane dehydrogenation.

1. Introduction

Shale gas revolution in North America has recently promoted the mass production of natural gas liquids, specifically ethane and propane, making on-purpose olefin production from alkane dehydrogenation an attractive alternative to the traditional olefin production processes, such as steam crackers and fluid catalytic cracking of naphtha, light diesel, and other oil byproducts [1,2]. Because of the economical

feedstock, relatively higher selectivity towards propylene, and lower energy demand, propane dehydrogenation (PDH) has become one of the most competitive propylene production processes and has already been successfully commercialized by Honeywell UOP (Oleflex), CB&I Lummus (Catofin), and Uhde (STAR).

Pt-based catalysts are among the most commonly used commercial catalysts for PDH [3], but they suffer from the unsatisfactory selectivity towards propylene and poor catalyst stability due to coke formation. The strongly exothermic nature of PDH [$C_3H_8(g) \rightleftharpoons C_3H_6(g) + H_2(g)$, $\Delta_r H^o = +123.8\,kJ/mol$] requires high reaction temperature (around 600 °C) to achieve a reasonable propane conversion. However, under such an operating condition, side reactions, such as hydrogenolysis, cracking, oligomerization, cylclization, and aromatization, are promoted even more dramatically, thus lowering the catalyst selectivity [4]. In the side reactions, propylene or other C3 species would be deeply dehydrogenated to give C1 and C2 species that may subsequently desorb to form ethane, ethylene, and methane or server as coke precursors [5]. The formation of coke could block the active sites of catalysts, impede the catalytic activity, and eventually deactivate the catalysts completely [6]. Therefore, the catalyst selectivity in PDH dictates not only the yield of propylene, but also plays a key role in determining the stability of the catalyst, and the development of Pt-based catalysts with improved selectivity and increased resistance to coke formation is highly desired.

To increase the selectivity toward propylene at relatively high catalytic activity, various attempts have been made to modify the geometric and electronic structures of the Pt-based catalysts [7–9]. First, novel preparation methods have been proposed to control the size and shape of Pt nanoparticles [10,11], which were believed to have a significant influence on the activity, selectivity, and stability of the catalysts. For example, it was reported that Pt clusters of small cluster sizes that are dominated by coordinatively unsaturated metal atoms on the surface have a lower dehydrogenation energy barrier and thus a higher catalytic activity, while on large Pt clusters with Pt(1 1 1) dominating a weakened binding strength of propylene (and hence an improved selectivity) result because the possibility of deep dehydrogenation is lowered [12]. Second, addition of a second metal, including Sn, Ga, Cu, Ir and In, to the platinum catalyst to form bimetallic catalysts is also an effective way to suppress undesired side reactions [13–17]. It was reported that the hydrogenolysis and isomerization reactions may be suppressed by doping Pt with Sn, because the dopant can selectively cover the under-coordinated platinum sites which are responsible for the side reactions [9]. Third, coke deposition via polymerization of deeply dehydrogenated species can be substantially reduced by using supports with little to no Brønsted acidity [18]. For instance, Xia et al. claimed that using Mg to dope the Al_2O_3 support gives rise to the spinel phase, which can promote the reduction of Pt species and inhibit coke formation. After 8 reaction-regeneration cycles, the initial and final propane conversions of 66.4% and 43.5% can still be attained, with the propylene selectivity of about 95% [19].

Near-surface alloys (NSAs), in which a solute metal is present as the overlayer or in the subsurface of a host metal, exhibit unique chemical and physical properties that are distinct from the properties of their constituent metals. It has been suggested that NSAs can represent a combination of weak atomic hydrogen binding and facile H_2 dissociation [20], thereby facilitating highly selective hydrogenation at low temperatures, and are therefore excellent candidates as electrocatalysts in fuel cells [21,22]. Core-shell alloys are NSAs that have a few layers of atoms of one metal enriching the shell of their nanoparticles and have another metal staying in the inner core. Experimentally, core-shell alloy catalysts can be synthesized in controlled environment in the atomic layer deposition and dendrimer encapsulation techniques [23,24]. Because of the size mismatch and electronegativity difference, the electronic structures of the shell atoms are modified by the core atoms through the combined strain and ligand effects [25], making it possible to tailor the adsorption and catalytic properties of the core-shell alloys to a particular application. Hwu et al. reported that the Ni@Pt core-shell catalyst can catalyze the cyclohexene hydrogenation reaction while the monometallic Pt and Ni do not have any catalytic activity [26]. In addition, the core-shell nanostructure provides an effective way of increasing the utilization efficiency of precious metals. The substitution of less expensive or non-precious metals for Pt in the core region can significantly increase the Pt dispersion and therefore reduce the catalyst cost. For example, Xie et al. claimed that the Pt dispersion of the Pd@Pt_{1L}/C catalyst is almost four times larger than that of the Pt nanocubes [27].

Despite some experimental work has been devoted to studying dehydrogenation reactions over core-shell alloy catalysts [26,28], a quantitative structure-activity relationship has not yet been established by correlating data on the activity of core-shell alloys with their electronic structures. In the current work, density functional theory (DFT) calculations and microkinetic analysis have been carried to identify Pt-based core-shell alloy catalysts with improved catalyst selectivity and coke resistance for propane dehydrogenation. The plane and stepped surfaces of 11 M@Pt (M = Fe, Co, Ni, Cu, Ru, Rh, Pd, Ag, Os, Ir, and Au) core-shell alloys are first constructed. Next, the electronic structures of surface Pt atoms are characterized upon substitution of late transition metals for the Pt atoms in the core region. Then, linear scaling relations are established to identify the descriptor that can be used to represent the overall reaction kinetics. Finally, using the derived linear scaling relations, we single out the best core-shell alloy catalyst for propane dehydrogenation that exhibits improved propylene selectivity and comparable catalytic activity.

2. Computational details

2.1. M@Pt surface model construction

The segregation energy (E_{seg}) is defined as the energy required to move a solute atom from the core to the surface of a host metal, which can be used to predict the surface composition of alloyed nanoparticles [20]. If E_{seg} is negative, then the surface would be dominated by the solute atoms and the overlayer configuration is more stable. In contrast, if E_{seg} is positive, then the surface layer would be dominated by the host atoms and the subsurface configuration is more stable [29]. The previously calculated E_{seg} indicated that, except for Cu, Pd, Ag, and Au, the segregation of Pt from the bulk to the surface of late transition metals is negative [30,31], meaning that Pt atoms prefer to stay on the shell of most M@Pt core-shell alloys. It is well known, however, that the surface structure and composition of nanoparticles can be modified in response to the change in reaction conditions. Tao et al. [32] observed an opposite segregation behavior of Rh and Pd under oxidizing and reducing conditions and suggested that the underlying reason lies in the fact that the Rh oxide is more stable than the Pd oxide, which provides a driving force for the segregation and preferential oxidation of Rh, whereas in an atmosphere of CO the reduced Pd has a lower surface energy and therefore enriches the shell. In propane dehydrogenation, propylene is obviously the most important chemisorbed species on the catalyst surface. Our calculated results indicate that among the 12 transition metals Pt binds propylene most strongly. By comparison, the heat of propylene adsorption on the Cu(1 1 1), Ag(1 1 1), and Au(1 1 1) surfaces are only less than 0.1 eV. Therefore, under realist experimental conditions, the surface free energy of Pt would be lowered to the largest extent by the adsorption of carbonaceous species, which in turn drives Pt atoms to the surface to form M@Pt core-shell nanoparticles.

The plane surfaces of the M@Pt core-shell nanoparticles are represented by five-layer slabs of Fe(1 0 0), Co(0001), Ni(1 1 1), Cu(1 1 1), Ru(0001), Rh(1 1 1), Pd(1 1 1), Ag(1 1 1), Os(0001), Ir(1 1 1), and Au(1 1 1) with a $p(3 \times 3)$ supercell, where the M atoms in the outermost layer are replaced with Pt atoms, as shown in Fig. 1a. The models of this type are commonly used to investigate the adsorption and catalytic behavior of the core-shell catalyst surfaces [33–35]. Upon

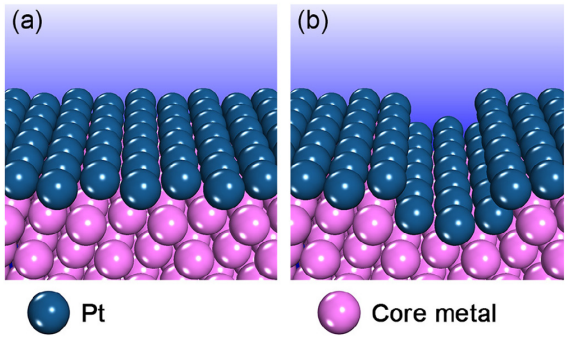

Fig. 1. Schematic representations of (a) plane and (b) stepped surfaces of M@Pt core-shell alloys.

substitution, the surface lattice constants are optimized by fully relaxing the alloyed slabs until the forces on each atom are less than 0.01 eV/Å. As a first test of our method, a sphere-like Ru@Pt core-shell nanoparticle with the diameter of 2 nm was also constructed. After geometry optimization, it was found that the Pt-Pt and Ru-Pt interatomic distances in the slab model are comparable with those in the cluster model. As for the stepped M@Pt core-shell surfaces, five-layer slabs in a rectangular ($3 \times 2\sqrt{3}$) supercell geometry are repeated periodically and defects are introduced by removing two rows of M metal atoms in the uppermost layer. Then, the Pt atoms were substituted for the M atoms in the exposed layer, as shown in Fig. 1b. The bottom two layers of both plane and stepped surfaces were fixed to their crystal lattice positions. The neighboring slabs were separated by a vacuum region as thick as 12 Å in the direction perpendicular to the surface to eliminate periodic interactions. The first Brillouin zones of the $p(3 \times 3)$ and rectangular ($3 \times 2\sqrt{3}$) supercells are sampled with Γ-centered $5 \times 5 \times 1$ and $2 \times 4 \times 1$ k-point grids, respectively.

2.2. DFT calculation

DFT calculations were performed by using the Vienna *ab-initio* simulation package (VASP) [36–38], where the interactions between valence electrons and ion cores are represented by pseudopotentials and the electronic wavefunctions at each k-point are expanded in terms of a discrete plane-wave basis set. Here we used Blöchl's all-electron-like projector augmented wave (PAW) method [39] as implemented by Kresse and Joubert [40]. Exchange and correlation effects were treated with the generalized gradient approximation (GGA) in the formulation of the Perdew-Burke-Ernzerhof (PBE) functional [41]. A plane wave energy cutoff of 400 eV was used in the present calculations and all geometries were optimized by using a force-based conjugate gradient algorithm [42] until the forces acting on each atom were converged better than 0.03 eV/Å. Brillouin zone sampling was performed by using a Monkhorst-Pack grid [43] and electronic occupancies were determined according to a Methfessel-Paxton scheme [44] with an energy smearing of 0.2 eV. Spin polarization was taken into account in calculations involving magnetic Fe, Co, and Ni. Transition states were located by using the dimer method [45] and validated with vibrational analysis.

2.3. Microkinetic analysis

In order to determine the catalytic activity of the M@Pt core-shell catalysts, the turnover frequency (TOF) for the dehydrogenation of propane was calculated at 793.15 K. The feed consists of 3 kPa propane, 3 kPa hydrogen, and 0.15 kPa propylene. The thermodynamic properties of gas-phase species, adsorbed intermediates, and activated complexes under relevant conditions were calculated in the ideal-gas and harmonic limits, and the details can be found in our previous work [46]. The rate constant for elementary steps was estimated on the basis of transition state theory (TST) [47], which is written as

$$k = (k_B T/h) \exp(S^{o\ddagger}/k_B T) \exp(-H^{o\ddagger}/k_B T) \tag{1}$$

where k is the rate constant, k_B Boltzmann's constant, h Planck's constant, $S^{o\ddagger}$ the entropy change from the initial to the transition state, $H^{o\ddagger}$ the enthalpy change from the initial to the transition state, and T the reaction temperature.

The TOFs for elementary steps were obtained by solving a mean-field microkinetic model to steady state. The differential equations can be expressed as

$$r_i = k_i^+ \prod_n \theta_{in} \prod_n p_{in} - k_i^- \prod_l \theta_{il} \prod_l p_{il} \tag{2}$$

$$\partial\theta_j/\partial t = \sum_i s_{ji} r_i \tag{3}$$

where r_i is the rate for each elementary step, k_i^+ the forward rate constant, k_i^- the reverse rate constant, θ_{in} and θ_{il} are the surface concentrations of the reactant and product for elementary step i, p_{in} and p_{il} are the unitless pressure of the gas-phase reactant and product for elementary step i, and s_{ji} is the stoichiometric coefficient of species j in elementary step i. This set of coupled non-linear ordinary differential equations has a steady-state solution as

$$\partial\theta_j/\partial t = 0 \tag{4}$$

which can be solved subject to the site conservation constraint:

$$\sum_j \theta_j = \theta^{TOT} \tag{5}$$

where θ^{TOT} is the normalized surface area.

3. Results and discussion

3.1. Reaction network for propane dehydrogenation

It is generally accepted that the dehydrogenation of propane over Pt catalyst follows the reverse Horiuti-Polanyi mechanism [48], in which the main elementary steps include the dissociative adsorption of propane on the catalyst surface, the cleavage of the second C—H bond to form propylene, and the final desorption of propylene and hydrogen. As stated in the Introduction, however, side reactions occur when propylene is deeply dehydrogenated. In principle, if the Gibbs free energy barrier for propylene desorption is lower than that for propylene dehydrogenation, propylene molecules could be readily released from the metal surface, thereby giving rise to a high propylene selectivity. Otherwise, propylene would be deeply dehydrogenated until formation of propyne is achieved, which is suggested to be the starting point for C—C bond breaking [8]. Thus, the selectivity issue arises from the competition between the propylene desorption and the deep dehydrogenation of propylene, and the difference in Gibbs free energy barrier between these two steps can be used to represent the catalyst selectivity toward propylene. Since the entropy and enthalpy of the activated complex in molecular adsorption or desorption compare closely to those of the adsorbed intermediate and gas-phase species [47], respectively, and because the entropy change for propylene dehydrogenation is usually negligible (less than 0.0002 eV/K under experimental conditions), the activation energy difference between propylene dehydrogenation and desorption can be used instead as the selectivity descriptor.

As demonstrated previously, propane and propylene dehydrogenation do not show any special preference for the organic group where the C—H bond is broken. The activation energy difference between the formation of 1- and 2-propyl is approximately 0.01 eV and, from a kinetic perspective, the dehydrogenation of propylene to 1- and 2-

propenyl is equally favorable [8,12]. For this reason, the reaction network can be simplified as

$$CH_3CH_2CH_3(g) + 2* \rightleftharpoons CH_3CH_2CH_2* + H* \quad (6)$$

$$CH_3CH_2CH_2* + * \rightleftharpoons CH_3CHCH_2* + H* \quad (7)$$

$$CH_3CHCH_2* \rightleftharpoons CH_3CHCH_2(g) + * \quad (8)$$

$$CH_3CHCH_2* + * \rightleftharpoons CH_3CHCH* + H* \quad (9)$$

$$2H* \rightleftharpoons H_2(g) + 2* \quad (10)$$

where * represents a free surface site and A* represents the species A adsorbed on the surface. In this scheme, the first C–H bond activation takes place at the $-CH_3$ group and the $-CH_2$ group in propylene is activated for the third H abstraction.

3.2. Adsorption properties of M@Pt core-shell alloys

In the simplified reaction network, the adsorption of propane and propylene on metal surfaces has been the subject of extensive research [8,49]. It is now generally agreed that there is no hybridization between propane and metal *d* states and propane is physisorbed on the metal surfaces [50]. Since standard GGA fails to account for long-range van der Waals interactions, a nonlocal correlation functional, the vdW-DF2 functional, was employed to predict the London dispersion forces between propane and transition metals, and the adsorption energy is calculated as

$$\Delta E_{ads}(propane) = E_{propane/surface} - E_{surface} - E_{propane} \quad (11)$$

where $E_{propane/surface}$ is the total energy of propane adsorbed on the surface, $E_{surface}$ is the total energy of the clean surface, and $E_{propane}$ is the total energy of the molecular propane. The calculated results given in Table 1 indicate that the adsorption energies of propane are in the range −0.31 to −0.37 eV and −0.37 to −0.50 eV on the plane and stepped surfaces, respectively, both of which are moderately sensitive to the identity of the core-shell alloy surface. Furthermore, the propane molecule experiences stronger attractive interaction from the stepped surface because there exists a larger contact area between them (see Fig. 2a and b) and the strength of dispersion forces tend to increase with increasing molecular size. To evaluate the reliability of the used computational method, the newly developed BEEF-vdW functional [51], which can simultaneously describe the long-range van der Waals interactions and short-range covalent bonding, is also employed to calculate the adsorption energies of propane on the metal surfaces (The data are given in Table S1). Comparison of the results by the two functionals indicates that both of them are capable of providing a reasonably accurate description of the interactions between propane and metal surfaces.

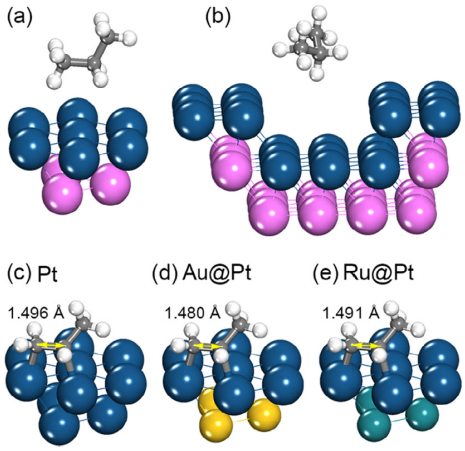

Fig. 2. Adsorption configurations of propane on both (a) plane and (b) stepped M@Pt surfaces and adsorption configurations of propylene on (c) Pt(1 1 1), (d) Au@Pt(1 1 1), and (e) Ru@Pt(1 1 1) surfaces.

Unlike propane, propylene is covalently adsorbed at the Bridge site between two Pt atoms on the both the plane and the stepped surfaces, which is known as the di-σ mode, and the optimized structures on the core-shell alloys resemble that on the Pt surface, except that the C=C double bond is shortened regardless of the metal enriching the core region, as shown in Fig. 2c–e. The adsorption energy of propylene and other C3 species can be calculated according to

$$\Delta E_{ads} = E_{C_3H_x/surface} - E_{surface} - E_{propylene} - (x/2)E_{hydrogen} \quad (12)$$

where $E_{C_3H_x/surface}$ is the total energy of the adsorbed intermediate or activated complex on the surface, $E_{propylene}$ the total energy of gas-phase propylene, and $E_{hydrogen}$ the total energy of gas-phase hydrogen. From Table 1 (The data obtained by using the BEEF-vdW functional are given in Table S1 for comparison), one can see that the binding strength of propylene to the metal surface varies greatly with the core metal. Since the lattice constant of Pt is different from that of the core metal, the Pt atoms on the shell would adopt the lattice constant of the respective substrate. Therefore, the interatomic distance between surface Pt atoms is typically different from that of monometallic Pt, leading to the lateral compression or stretching of the Pt monolayer compared to bulk Pt, as indicated in Table 1. The strain effect would modify the electronic structure of the surface metal by changing the overlap between *d* orbitals and thus affect the adsorption and catalytic properties of the active surface [52]. On the other hand, the adsorption behavior of the

Table 1
Calculated adsorption energies of propane and propylene and electronic and geometric structures on M@Pt surfaces.

Surface	ΔE_{ads}(propane) (eV)		ΔE_{ads}(propylene) (eV)		$d_{Pt\text{-}Pt}$ (Å)	Bader charge (electrons/atom)	ε_d[a] (eV)
	Terrace	Step	Terrace	Step			
Fe@Pt	−0.33	−0.37	0.08	−0.87	2.59	10.27	−2.61
Co@Pt	−0.33	−0.44	−0.03	−0.94	2.58	10.19	−2.57
Ni@Pt	−0.31	−0.39	−0.32	−1.12	2.58	10.17	−2.36
Cu@Pt	−0.36	−0.40	−0.11	−1.15	2.63	10.19	−2.17
Ru@Pt	−0.37	−0.44	−0.30	−0.95	2.71	10.16	−2.72
Rh@Pt	−0.32	−0.47	−0.50	−1.14	2.70	10.11	−2.48
Pd@Pt	−0.32	−0.49	−1.01	−1.40	2.75	10.08	−1.87
Ag@Pt	−0.33	−0.43	−0.51	−1.08	2.84	10.15	−1.57
Os@Pt	−0.31	−0.49	−0.45	−0.95	2.73	10.16	−2.70
Ir@Pt	−0.31	−0.50	−0.59	−1.19	2.72	10.09	−2.57
Pt	−0.31	−0.46	−1.08	−1.41	2.82	10.05	−1.93
Au@Pt	−0.31	−0.42	−0.83	−1.33	2.85	10.07	−1.58

[a] *d*-band center.

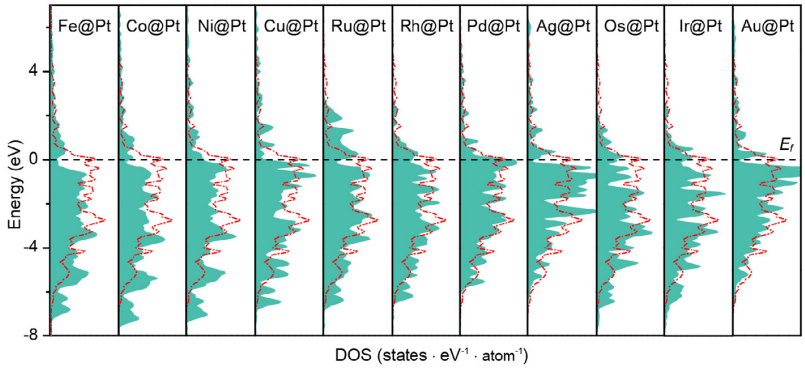

Fig. 3. Calculated density of states (DOSs) projected onto the *d* orbital of the Pt atoms in outermost layer of the M@Pt plane surfaces (shaded in green) and Pt(1 1 1) surface (red line).

core-shell alloy surfaces is determined not only by the strain effect but also by the electron transfer between the solute and host metal, which is known as the ligand effect and arises from the change in the chemical environment of a metal with its surrounding ligand [25].

Typically, the trend in the adsorption energy of small molecules on transition metals can be rationalized according to the *d*-band model proposed by Hammer and Nørskov [53]. In this model, the *d*-band filling is assumed to be conserved (see Table S2) and the *d*-band width is the key factor that influences the *d*-band center. When the Pt overlayer is compressed, the overlap between the *d*-orbitals from the adjacent Pt atoms increases, which broadens the *d*-band and leads to a downshift in the *d*-band center (ε_d). Conversely, when the Pt overlayer is stretched, the *d* orbital overlap is reduced, leading to a narrowed *d*-band and giving rise to an upshift in ε_d [54,55]. For instance, as shown in Fig. 3, the *d*-band of Pt atoms in Au@Pt is narrowed and becomes sharper than that of monometallic Pt. As a result, the *d*-band center needs to move up to conserve the *d*-band filling. It can be seen from Table 1 that the interatomic distances between the nearest neighbor Pt atoms on the Au substrate is longer than that on Pt(1 1 1) and, consequently, an upshift of 0.35 eV in ε_d results. By comparison, the Pt-Pt bond length in the Ru@Pt core-shell alloy is shortened due to the smaller atomic size of Ru, leading to a downshift of 0.79 eV in ε_d. It is important to note that apart from the strain effect, the charge transfer between the solute and host metal can also affect the energy of the *d*-band of the Pt atoms on the shell. On the basis of the Bader charge analysis [56], one can see that there is a considerable electron transfer from the host to the solute Pt. However, further electronic structure analysis indicates that the population of electrons in the Pt *d* orbital does not change. Instead, the transferred electrons are found to fill the *s* and *p* orbitals of Pt and thus shift the *d*-band center by changing the *d*-band shape (The details are included in the Supporting Information).

According to the *d*-band model [53], downshifting the ε_d of surface atoms would reduce the interaction strength between the surface and adsorbates, whereas upshifting the ε_d of surface atoms may cause the antibonding states to, at least in part, shift up through the Fermi level and become empty, which eventually leads to a stronger binding strength of the adsorbate to the metal surface. When the 3*d*-block transition metals serve as the core element, for instance, the ε_d of the Pt atoms on the Cu@Pt surfaces is closest to the Fermi level while the *d*-band of the Pt atoms on the Fe@Pt is shifted farthest below the Fermi level. As a consequence, the interaction between the Cu@Pt surface and propylene is much stronger than that between Fe@Pt and propylene. The positive adsorption energy on Fe@Pt(1 1 1) is due to the significant surface reconstruction upon propylene adsorption.

Furthermore, the calculated adsorption energies of propylene also indicate that the coordinatively unsaturated surface sites are generally more reactive for propylene adsorption than the plane surface, which can be explained by the lower coordination number (and hence the higher *d*-band energy) of the Pt atoms on the stepped surface [57]. Compared with the plane surface, the stepped surface could dramatically enhance the binding strength of propylene, which is reflected in its increased adsorption heat. On the other hand, propylene is more difficult to desorb from the stepped surface than from the plane surface. It is therefore reasonable to expect that the propylene selectivity on the stepped surfaces is lower than that on the plane surfaces.

The other C3 species in the simplified reaction network include 1-propyl and 1-propenyl, which can also be chemisorbed on both the plane and the stepped core-shell surfaces, where 1-propyl prefers to be bound at the Atop site while 1-propenyl tends to be adsorbed at the FCC site. The calculated adsorption energies of 1-propyl and 1-propenyl are summarized in Table S3 and plotted against the adsorption energy of propylene, as shown in Fig. 4. It is clear from the figure that very good linear scaling relations are established, which can be explained by the fact that the adsorption energies of different surface intermediates that are bound to the metal surface via the same atom generally scale with each other [58]. Furthermore, according to the bond order conservation model, Jones et al. suggested that the adsorption energies of C_2H_x-type adsorbates on transition metal surfaces should scale with each other [59]. It is therefore not surprising to learn that the adsorption of 1-propy, propylene, and 1-propeynyl that have different degrees of unsaturation is governed by the same physics.

3.3. Energetics of propane dehydrogenation

The energy profiles for propane dehydrogenation and propylene deep dehydrogenation over the M@Pt plane and stepped surfaces are shown in Fig. 5, where the abstracted hydrogen atoms are believed to be able to diffuse quickly to a position that is infinitely far from the remaining C3 species, and the activation energies for the three dehydrogenation elementary steps are summarized in Table 2. From the figure, one can see that on Pt(1 1 1), the dehydrogenation of propane is kinetically more favorable than the activation of the second C—H bond but the enthalpy change for 1-propyl dehydrogenation is more negative than the first C—H bond activation, implying that the second dehydrogenation step is thermodynamically more favorable. On the stepped surface, the two dehydrogenation steps have almost the same energy barrier and much more negative energy change than those on the plane surface, which agrees well with the previously proposed size-dependent reaction mechanism and kinetics for propane dehydrogenation [12].

When the core metal is changed from Pt to the other late transition metals, it is found that the energy profiles are all shifted upward because the binding strength of the C3 species is generally weakened on M@Pt compared to that on Pt. For bond-breaking reactions, the energy of the final state is increased more dramatically than the initial state

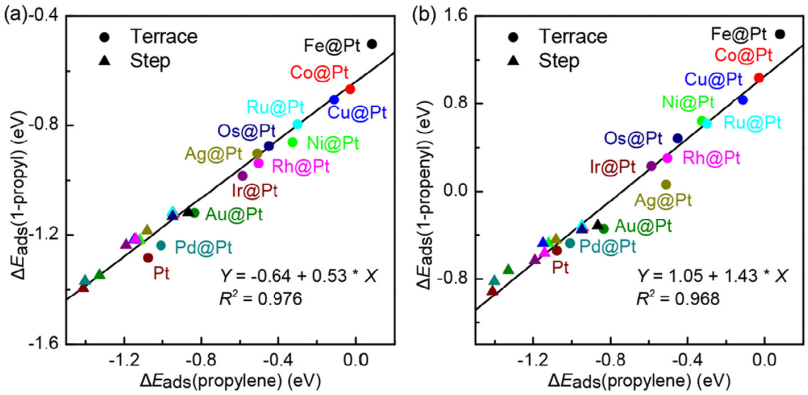

Fig. 4. Chemisorption energy scaling relations between the adsorption energies of (a) 1-propyl and (b) 1-propenyl and propylene.

owing to the surface-mediated bonding competition effect [53], thereby leading to a less negative or more positive energy change, which in turn causes the energy profiles to become less "downhill" or even "uphill". In addition, considering the Brønsted-Evans-Polanyi (BEP) relationship which states that the activation energy for an elementary step scales linearly with the reaction heat [60–62], the propane dehydrogenation activity would be decreased with increasing the activation energy, while the side reaction, namely, the deep dehydrogenation of propylene, would be simultaneously suppressed, resulting in a better propylene selectivity.

3.4. *Transition state energy scaling relations in propane dehydrogenation*

Since the activation energy for the elementary steps also varies with the core metal, it is would be interesting to see if there exists a simple descriptor that can be used to represent the energy of the transition states. Before identifying a single descriptor, we first plotted the energies of the transition states against the energies of their respective final states, as suggested by the BEP relationship. One can see in Fig. 6a–c that the scaling between these two quantities gives very good straight lines. Interestingly, essentially the same linear scaling relation is found for both the plane and the stepped surfaces, which can be explained by the weak geometry dependence of the dehydrogenation reactions [63]. It is also found that the data on the stepped surfaces are positioned at the bottom left of those on the plane surfaces, so their displacement along the BEP lines is indicative of the electronic effect. In addition, the slope of these linear scaling relations is close to 1,

Table 2
Calculated energy barriers (E_{act}) for propane dehydrogenation and propylene deep dehydrogenation over M@Pt plane and stepped surfaces.

Surface	E_{act}(propane deh) (eV)		E_{act}(1-propyl deh) (eV)		E_{act}(propylene deh) (eV)	
	Terrace	Step	Terrace	Step	Terrace	Step
Fe@Pt	1.65	0.75	1.38	0.57	1.67	0.57
Co@Pt	1.57	0.76	1.43	0.56	1.62	0.76
Ni@Pt	1.37	0.62	1.34	0.56	1.56	0.85
Cu@Pt	1.43	0.66	1.35	0.60	1.54	0.90
Ru@Pt	1.23	0.63	1.11	0.51	1.28	0.67
Rh@Pt	1.10	0.51	1.08	0.41	1.19	0.64
Pd@Pt	0.71	0.38	0.77	0.36	0.87	0.73
Ag@Pt	0.98	0.63	0.90	0.55	0.97	0.85
Os@Pt	1.10	0.62	1.02	0.48	1.23	0.61
Ir@Pt	1.03	0.44	1.01	0.34	1.12	0.56
Pt	0.59	0.27	0.66	0.27	0.71	0.50
Au@Pt	0.77	0.41	0.77	0.56	0.80	0.73

signifying that the optimized structures of the transition states resemble those of the final states, as shown in Fig. 7.

As aforementioned, there is a good linear scaling relation between the adsorption energy of propylene and that of the other C3 species over the M@Pt core-shell alloys. On the basis of this information, the transition state scaling relations are established in terms of the adsorption energy of propylene and depicted in Fig. 6e, f. The good straight lines indicate that this quantity can be used as a descriptor to represent the

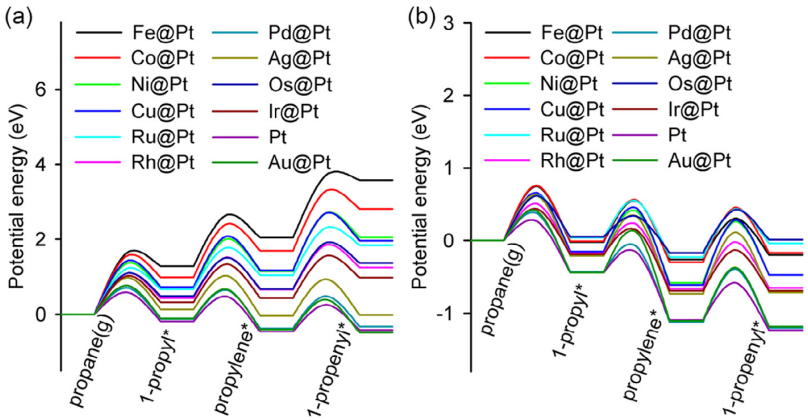

Fig. 5. Energy profiles for propane dehydrogenation and propylene deep dehydrogenation over M@Pt (a) plane and (b) stepped surfaces.

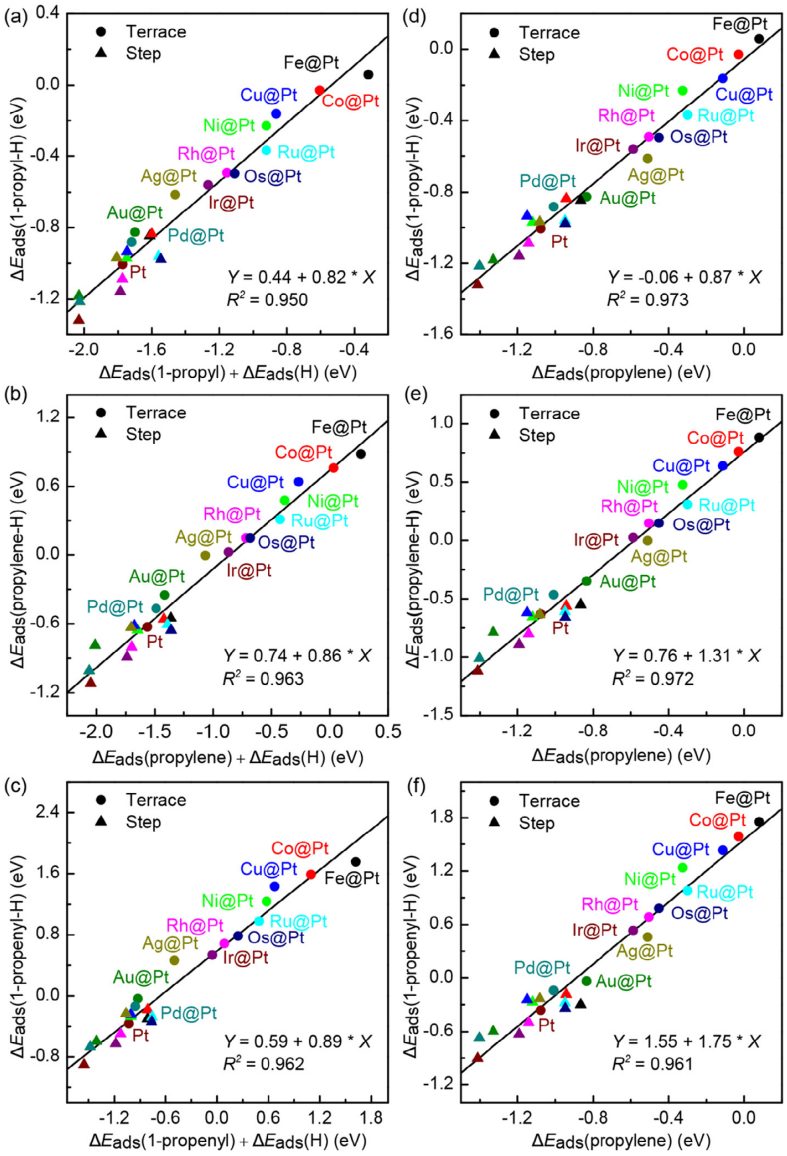

Fig. 6. Linear transition state energy scaling relations for (a, d) dehydrogenation of propane, (b, e) dehydrogenation of 1-propyl, and (c, f) deep dehydrogenation of propylene over 12 M@Pt surfaces.

energies of the other C3 species and transition states and can therefore describe the kinetics of propane dehydrogenation over M@Pt core-shell alloys.

3.5. *Rational catalyst screening for propane dehydrogenation*

While Pt is the most widely used catalyst for propane dehydrogenation, coke is readily formed on the catalyst surface at high temperatures and leads to rapid catalyst deactivation. Although the catalysts can be regenerated under oxidizing or oxychlorination conditions followed by hydrogen reduction, the catalytic performance may not be fully restored [64]. Moreover, the high cost and finite abundance is another important factor limiting the use of platinum catalysts. Therefore, it is highly desired to develop and apply novel catalysts with lower price and higher catalytic performance.

The recently developed descriptor-based microkinetic analysis combined with the DFT results provides an effective way of improving the understanding of trends in heterogeneous catalysis [65,66] and screening solid catalysts for catalytic reactions [58,67]. By using the concept of descriptors, the complex reaction kinetics can be described by a few simple variables. The search for the descriptors on heterogeneous catalyst surfaces is based on the chemisorption energy and transition state energy scaling relations. Apart from the adsorption energy of carbon which is the best known and most widely used descriptor, the adsorption energies of some other reaction intermediates can also be employed. For example, the methyl adsorption energy has been successfully used to describe the activity of selective acetylene hydrogenation [68].

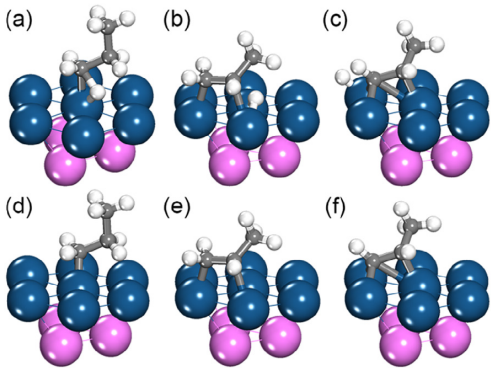

Fig. 7. Adsorption configurations of the transition states for (a) propane dehydrogenation, (b) 1-propyl dehydrogenation, and (c) propylene deep dehydrogenation and adsorption configurations of (d) 1-propyl, (e) propylene, and (f) 1-propenyl on M@Pt plane surfaces.

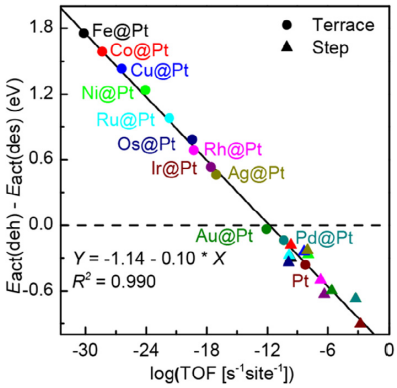

Fig. 9. Linear scaling relation between catalytic activity and selectivity for propane dehydrogenation over 12 core-shell alloy catalysts.

Given that the propylene adsorption energy has been identified as the descriptor in this work, it is not surprising that the turnover frequency for propane dehydrogenation has a good linear relationship with the propylene adsorption energy, as shown in Fig. 8a. A more negative value for the descriptor gives rise to a higher propane dehydrogenation rate. Furthermore, it is interesting to find that selectivity descriptor, namely, the activation energy difference between propylene dehydrogenation and desorption, also scales linearly with the adsorption energy of propylene, as shown in Fig. 8b. A stronger binding strength of propylene to the metal surface would not only promote the deep dehydrogenation but also hinder the desorption of propylene, thereby resulting in a more negative selectivity descriptor that is indicative of a lower propylene selectivity. From these two scaling relations, it follows that both the propylene yield and the catalyst stability are significantly affected by the adsorption energy of propylene on the metal surfaces.

To understand better the relationship between the catalytic activity and selectivity in propane dehydrogenation, the selectivity descriptor was plotted against the natural logarithm of the TOF, as shown in Fig. 9. From the figure, one can see that the catalyst selectivity toward propylene is lowered as the catalytic activity is increased. While Pt exhibits the highest catalytic activity for propane dehydrogenation, its selectivity is the lowest. In other words, the catalytic activity and propylene selectivity are negatively correlated, which helps explain why in experiment a higher catalyst selectivity can only be achieved at the expense of a lower catalytic activity.

Since catalyst nanoparticles are surrounded by both plane and stepped surfaces and the activity of the stepped surfaces would always dominate the overall reaction rate, the candidate catalysts were screened on the basis of the catalytic activity and selectivity of the stepped surface. Of the 11 M@Pt core-shell catalysts, one can see that Co@Pt is the best catalyst for the PDH reaction if a compromise is made between catalytic activity and selectivity. In experiment, the Co@Pt catalyst has already been synthesized utilizing a polyol reduction process and was found to show better catalytic performance toward the hydrolysis of NH_3BH than Pt and Pt_3Co [69]. However, the reasoning behind the experimental observation is still an open question. Our theoretical interpretation of the relationship between the catalytic activity and selectivity of the Pt-based surfaces provides important clues for the design of effective catalysts for propane dehydrogenation, yet further experimental work is highly desired to validate the prediction about the Co@Pt nanoparticle as a possible catalyst with improved propylene selectivity and coke resistance.

4. Conclusions

DFT calculations and microkinetic analysis have been carried out to explore the reaction kinetics of propane dehydrogenation over 11 M@Pt (M = Fe, Co, Ni, Cu, Ru, Rh, Pd, Ag, Os, Ir, and Au) core-shell catalysts. The adsorption and catalytic properties of the surface Pt atoms can be tuned by substituting late transition metals for the Pt atoms in the core region, which modifies the electronic structure of metal surfaces through the strain effect and electron transfer. Both the chemisorption energy and transition state energy scaling relations indicate that the adsorption energy of propylene can be used as a descriptor to

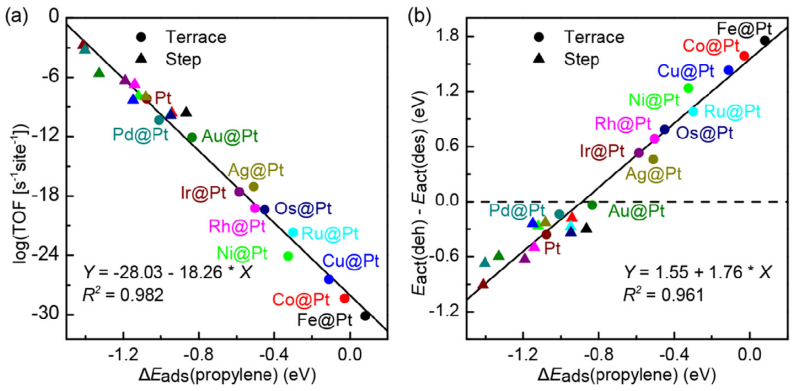

Fig. 8. Plots of adsorption energy of propylene against (a) TOF and (b) propylene selectivity descriptor (the activation energy difference between propylene dehydrogenation and desorption) for propane dehydrogenation over 12 M@Pt core-shell alloy catalysts at 793.15 K, 0.03 bar propane, 0.03 bar hydrogen, and 0.0015 bar propylene.

represent the energies of the other C3 species and transition states and can therefore describe the kinetics of propane dehydrogenation over M@Pt core-shell alloys. The scaling relations also suggest that a higher catalyst selectivity toward propylene can only be achieved at the expense of a lower catalytic activity for propane dehydrogenation. The core-shell catalysts are found to have less negative propylene adsorption energies and higher activation energies for the dehydrogenation reactions than Pt, thus giving rise to a lower catalytic activity and a higher selectivity toward propylene. If a compromise is made between catalytic activity and catalyst selectivity, Co@Pt is proposed to be the best core-shell catalyst for propane dehydrogenation. The scaling relations established in this work offer an opportunity to single out promising PDH catalysts with improved selectivity and coke resistance.

Acknowledgements

This work is supported by the Natural Science Foundation of China, China (91645122, 21473053, and U1663221), the National Key Research and Development Program of China, China (2018YFB0604700), and the Fundamental Research Funds for the Central Universities, China (222201718003). The computational time provided by the Notur project is highly acknowledged.

Appendix A. Supplementary data

Supplementary data to this article can be found online at https://doi.org/10.1016/j.cej.2018.09.210.

References

[1] P.C.A. Bruijnincx, B.M. Weckhuysen, Shale gas revolution: An opportunity for the production of biobased chemicals? Angew. Chem. Int. Ed. 52 (2013) 11980–11987.
[2] E. McFarland, Unconventional chemistry for unconventional natural gas, Science 338 (2012) 340–342.
[3] Z. Nawaz, Light alkane dehydrogenation to light olefin technologies: a comprehensive review, Rev. Chem. Eng. 31 (2015) 413–436.
[4] J. Im, M. Choi, Physicochemical stabilization of Pt against sintering for a dehydrogenation catalyst with high activity, selectivity, and durability, ACS Catal. 6 (2016) 2819–2826.
[5] S. Saerens, M.K. Sabbe, V.V. Galvita, E.A. Redekop, M.-F. Reyniers, G.B. Marin, The positive role of hydrogen on the dehydrogenation of propane on Pt(111), ACS Catal. 7 (2017) 7495–7508.
[6] Z. Lian, S. Ali, T. Liu, C. Si, B. Li, D.S. Su, Revealing the janus character of the coke precursor in the propane direct dehydrogenation on Pt catalysts from a kMC simulation, ACS Catal. 8 (2018) 4694–4704.
[7] J.J. Sattler, J. Ruiz-Martinez, E. Santillan-Jimenez, B.M. Weckhuysen, Catalytic dehydrogenation of light alkanes on metals and metal oxides, Chem. Rev. 114 (2014) 10613–10653.
[8] M.-L. Yang, Y.-A. Zhu, C. Fan, Z.-J. Sui, D. Chen, X.-G. Zhou, DFT study of propane dehydrogenation on Pt catalyst: effects of step sites, Phys. Chem. Chem. Phys. 13 (2011) 3257–3267.
[9] M.-L. Yang, Y.-A. Zhu, X.-G. Zhou, Z.-J. Sui, D. Chen, First-principles calculations of propane dehydrogenation over PtSn catalysts, ACS Catal. 2 (2012) 1247–1258.
[10] M.-L. Yang, J. Zhu, Y.-A. Zhu, Z.-J. Sui, Y.-D. Yu, X.-G. Zhou, D. Chen, Tuning selectivity and stability in propane dehydrogenation by shaping Pt particles: a combined experimental and DFT study, J. Mol. Catal. A Chem. 395 (2014) 329–336.
[11] Y. Zhu, Z. An, H. Song, X. Xiang, W. Yan, J. He, Lattice-confined Sn (IV/II) stabilizing raft-like Pt clusters: high selectivity and durability in propane dehydrogenation, ACS Catal. 7 (2017) 6973–6978.
[12] J. Zhu, M.-L. Yang, Y. Yu, Y.-A. Zhu, Z.J. Sui, X. Zhou, A. Holmen, D. Chen, Size-dependent reaction mechanism and kinetics for propane dehydrogenation over Pt catalyst, ACS Catal. 5 (2015) 6310–6319.
[13] H.N. Pham, J.J. Sattler, B.M. Weckhuysen, A.K. Datye, Role of Sn in the regeneration of Pt/γ-Al_2O_3 light alkane dehydrogenation catalysts, ACS Catal. 6 (2016) 2257–2264.
[14] G. Wang, H. Zhang, H. Wang, Q. Zhu, C. Li, H. Shan, The role of metallic Sn species in catalytic dehydrogenation of propane: Active component rather than only promoter, J. Catal. 344 (2016) 606–608.
[15] J. Wu, S.M. Sharada, C. Ho, A.W. Hauser, M. Head-Gordon, A.T. Bell, Ethane and propane dehydrogenation over PtIr/Mg(Al)O, Appl. Catal. A: Gen. 506 (2015) 25–32.
[16] T. Wang, F. Jiang, G. Liu, L. Zeng, Z.j. Zhao, J. Gong,, Effects of Ga doping on Pt/CeO_2-Al_2O_3 catalysts for propane dehydrogenation, AIChE J. 62 (2016) 4365–4376.
[17] Z. Han, S. Li, F. Jiang, T. Wang, X. Ma, J. Gong, Propane dehydrogenation over Pt-Cu bimetallic catalysts: the nature of coke deposition and the role of copper, Nanoscale 6 (2014) 10000–10008.
[18] J. Liu, Y. Yue, H. Liu, Z. Da, C. Liu, A. Ma, J. Rong, D. Su, X. Bao, H. Zheng, Origin of the robust catalytic performance of nanodiamond-graphene-supported Pt nanoparticles used in the propane dehydrogenation reaction, ACS Catal. 7 (2017) 3349–3355.
[19] K. Xia, W.-Z. Lang, P.-P. Li, L.-L. Long, X. Yan, Y.-J. Guo, The influences of Mg/Al molar ratio on the properties of PtIn/Mg(Al)O-x catalysts for propane dehydrogenation reaction, Chem. Eng. J. 284 (2016) 1068–1079.
[20] J. Greeley, M. Mavrikakis, Alloy catalysts designed from first principles, Nat. Mater. 3 (2004) 810.
[21] S. Praserthdam, P.B. Balbuena, Effects of oxygen coverage, catalyst size, and core composition on Pt-alloy core-shell nanoparticles for oxygen reduction reaction, Catal. Sci. Technol. 6 (2016) 5168–5177.
[22] H. Kim, M. Achermann, L.P. Balet, J.A. Hollingsworth, V.I. Klimov, Synthesis and characterization of Co/CdSe core/shell nanocomposites: bifunctional magnetic-optical nanocrystals, J. Am. Chem. Soc. 127 (2005) 544–546.
[23] Y. Lei, B. Liu, J. Lu, R.J. Lobo-Lapidus, T. Wu, H. Feng, X. Xia, A.U. Mane, J.A. Libera, J.P. Greeley, Synthesis of Pt-Pd core-shell nanostructures by atomic layer deposition: application in propane oxidative dehydrogenation to propylene, Chem. Mater. 24 (2012) 3525–3533.
[24] O.M. Wilson, R.W.J. Scott, J.C. Garcia-Martinez, R.M. Crooks, Synthesis, characterization, and structure-selective extraction of 1–3 nm diameter AuAg dendrimer-encapsulated bimetallic nanoparticles, J. Am. Chem. Soc. 127 (2005) 1015–1024.
[25] J. Kitchin, J.K. Nørskov, M. Barteau, J. Chen, Modification of the surface electronic and chemical properties of Pt(111) by subsurface 3d transition metals, J. Chem. Phys. 120 (2004) 10240–10246.
[26] H.H. Hwu, J. Eng, J.G. Chen, Ni/Pt(111) bimetallic surfaces: unique chemistry at monolayer Ni coverage, J. Am. Chem. Soc. 124 (2002) 702–709.
[27] S. Xie, S.-I. Choi, N. Lu, L.T. Roling, J.A. Herron, L. Zhang, J. Park, J. Wang, M.J. Kim, Z. Xie, M. Mavrikakis, Y. Xia, Atomic layer-by-layer deposition of Pt on Pd nanocubes for catalysts with enhanced activity and durability toward oxygen reduction, Nano Lett. 14 (2014) 3570–3576.
[28] C. Xu, B.E. Koel, Dehydrogenation of cyclohexene on ordered Sn/Pt(111) surface alloys, Surf. Sci. 304 (1994) 249–266.
[29] Z. Zhao, G. Lu, Computational screening of near-surface alloys for CO_2 electroreduction, ACS Catal. 8 (2018) 3885–3894.
[30] L.-L. Wang, D.D. Johnson, Predicted trends of core-shell preferences for 132 late transition-metal binary-alloy nanoparticles, J. Am. Chem. Soc. 131 (2009) 14023–14029.
[31] A.V. Ruban, H.L. Skriver, J.K. Nørskov, Surface segregation energies in transition-metal alloys, Phys. Rev. B 59 (1999) 15990–16000.
[32] F. Tao, M.E. Grass, Y. Zhang, D.R. Butcher, J.R. Renzas, Z. Liu, J.Y. Chung, B.S. Mun, M. Salmeron, G.A. Somorjai, Reaction-driven restructuring of Rh-Pd and Pt-Pd core-shell nanoparticles, Science 322 (2008) 932–934.
[33] A.U. Nilekar, S. Alayoglu, B. Eichhorn, M. Mavrikakis, Preferential CO oxidation in hydrogen: reactivity of core-shell nanoparticles, J. Am. Chem. Soc. 132 (2010) 7418–7428.
[34] V. Pallassana, M. Neurock, L.B. Hansen, B. Hammer, J.K. Nørskov, Theoretical analysis of hydrogen chemisorption on Pd(111), Re(0001) and Pd_{ML}/Re(0001), Re_{ML}/Pd(111) pseudomorphic overlayers, Phys. Rev. B. 60 (1999) 6146–6154.
[35] S. Alayoglu, A.U. Nilekar, M. Mavrikakis, B. Eichhorn, Ru-Pt core-shell nanoparticles for preferential oxidation of carbon monoxide in hydrogen, Nat. Mater. 7 (2008) 333–338.
[36] G. Kresse, J. Hafner, Ab initio molecular dynamics for liquid metals, Phys. Rev. B 47 (1993) 558–561.
[37] G. Kresse, J. Furthmüller, Efficiency of ab-initio total energy calculations for metals and semiconductors using a plane-wave basis set, Comp. Mater. Sci. 6 (1996) 15–50.
[38] G. Kresse, J. Furthmüller, Efficient iterative schemes for ab initio total-energy calculations using a plane-wave basis set, Phys. Rev. B 54 (1996) 11169–11186.
[39] P.E. Blöchl, Projector augmented-wave method, Phys. Rev. B 50 (1994) 17953–17979.
[40] G. Kresse, D. Joubert, From ultrasoft pseudopotentials to the projector augmented-wave method, Phys. Rev. B 59 (1999) 1758–1775.
[41] J.P. Perdew, K. Burke, M. Ernzerhof, Generalized gradient approximation made simple, Phys. Rev. Lett. 77 (1996) 3865–3868.
[42] D. Sheppard, R. Terrell, G. Henkelman, Optimization methods for finding minimum energy paths, J. Chem. Phys. 128 (2008) 134106.
[43] H.J. Monkhorst, J.D. Pack, Special points for brillouin-zone integrations, Phys. Rev. B 13 (1976) 5188–5192.
[44] M. Methfessel, A.T. Paxton, High-precision sampling for brillouin-zone integration in metals, Phys. Rev. B 40 (1989) 3616–3621.
[45] G. Henkelman, H. Jónsson, A dimer method for finding saddle points on high dimensional potential surfaces using only first derivatives, J. Chem. Phys. 111 (1999) 7010–7022.
[46] Y.-A. Zhu, D. Chen, X.-G. Zhou, W.-K. Yuan, DFT studies of dry reforming of methane on Ni catalyst, Catal. Today 148 (2009) 260–267.
[47] R.D. Cortright, J.A. Dumesic, Kinetics of heterogeneous catalytic reactions: analysis of reaction schemes, Adv. Catal. 46 (2001) 161–264.
[48] I. Horiuti, M. Polanyi, Exchange reactions of hydrogen on metallic catalysts, Trans. Faraday Soc. 30 (1934) 1164–1172.
[49] M.-L. Yang, Y.-A. Zhu, C. Fan, Z.-J. Sui, D. Chen, X.-G. Zhou, Density functional study of the chemisorption of C_1, C_2 and C_3 intermediates in propane dissociation on Pt(111), J. Mol. Catal. A: Chem. 321 (2010) 42–49.
[50] L. Nykänen, K. Honkala, Density functional theory study on propane and propene adsorption on Pt(111) and PtSn alloy surfaces, J. Phys. Chem. C 115 (2011)

9578–9586.
[51] J. Wellendorff, K.T. Lundgaard, A. Møgelhøj, V. Petzold, D.D. Landis, J.K. Nørskov, T. Bligaard, K.W. Jacobsen, Density functionals for surface science: exchange-correlation model development with Bayesian error estimation, Phys. Rev. B 85 (2012) 235149.
[52] R.R. Adzic, J. Zhang, K. Sasaki, M.B. Vukmirovic, M. Shao, J.X. Wang, A.U. Nilekar, M. Mavrikakis, J.A. Valerio, F. Uribe, Platinum monolayer fuel cell electrocatalysts, Top. Catal. 46 (2007) 249–262.
[53] B. Hammer, J.K. Nørskov, Theoretical surface science and catalysis-calculations and concepts, Adv. Catal. 45 (2000) 71–129.
[54] A. Ruban, B. Hammer, P. Stoltze, H.L. Skriver, J.K. Nørskov, Surface electronic structure and reactivity of transition and noble metals1, J. Mol. Catal. A Chem. 115 (1997) 421–429.
[55] M. Mavrikakis, B. Hammer, J.K. Nørskov, Effect of strain on the reactivity of metal surfaces, Phys. Rev. Lett. 81 (1998) 2819.
[56] G. Henkelman, A. Arnaldsson, H. Jónsson, A fast and robust algorithm for Bader decomposition of charge density, Comp. Mater. Sci. 36 (2006) 354–360.
[57] B. Hammer, O.H. Nielsen, J.K. Nrskov, Structure sensitivity in adsorption: CO interaction with stepped and reconstructed Pt surfaces, Catal. Lett. 46 (1997) 31–35.
[58] F. Abild-Pedersen, J. Greeley, F. Studt, J. Rossmeisl, T. Munter, P.G. Moses, E. Skulason, T. Bligaard, J.K. Nørskov, Scaling properties of adsorption energies for hydrogen-containing molecules on transition-metal surfaces, Phys. Rev. Lett. 99 (2007) 016105.
[59] G. Jones, F. Studt, F. Abild-Pedersen, J.K. Nørskov, T. Bligaard, Scaling relationships for adsorption energies of C2 hydrocarbons on transition metal surfaces, Chem. Eng. Sci. 66 (2011) 6318–6323.
[60] T. Bligaard, J.K. Nørskov, S. Dahl, J. Matthiesen, C.H. Christensen, J. Sehested, The brønsted-evans-polanyi relation and the volcano curve in heterogeneous catalysis, J. Catal. 224 (2004) 206–217.
[61] M. Evans, M. Polanyi, Inertia and driving force of chemical reactions, Trans. Faraday Soc. 34 (1938) 11–24.
[62] J.N. Brønsted, Acid and basic catalysis, Chem. Rev. 5 (1928) 231–338.
[63] J.K. Nørskov, T. Bligaard, B. Hvolbæk, F. Abild-Pedersen, I. Chorkendorff, C.H. Christensen, The nature of the active site in heterogeneous metal catalysis, Chem. Soc. Rev. 37 (2008) 2163–2171.
[64] C. Sun, J. Luo, M. Cao, P. Zheng, G. Li, J. Bu, Z. Cao, S. Chen, X. Xie, A comparative study on different regeneration processes of Pt-Sn/γ-Al_2O_3 catalysts for propane dehydrogenation, J. Energy Chem. 27 (2018) 311–318.
[65] A. Vojvodic, J.K. Nørskov, New design paradigm for heterogeneous catalysts, Natl. Sci. Rev. 2 (2015) 140–143.
[66] J.K. Nørskov, T. Bligaard, J. Rossmeisl, C.H. Christensen, Towards the computational design of solid catalysts, Nat. Chem. 1 (2009) 37–46.
[67] S. Wang, V. Petzold, V. Tripkovic, J. Kleis, J.G. Howalt, E. Skulason, E. Fernandez, B. Hvolbæk, G. Jones, A. Toftelund, Universal transition state scaling relations for (de)hydrogenation over transition metals, Phys. Chem. Chem. Phys. 13 (2011) 20760–20765.
[68] F. Studt, F. Abild-Pedersen, T. Bligaard, R.Z. Sørensen, C.H. Christensen, J.K. Nørskov, Identification of non-precious metal alloy catalysts for selective hydrogenation of acetylene, Science 320 (2008) 1320–1322.
[69] X. Yang, F. Cheng, Z. Tao, J. Chen, Hydrolytic dehydrogenation of ammonia borane catalyzed by carbon supported Co core-Pt shell nanoparticles, J. Power Sour. 196 (2011) 2785–2789.